Accepted manuscript

1   **Optimizing Fenton-like process, homogeneous at neutral pH for Ciprofloxacin Degradation:**

2   **Comparing RSM-CCD and ANN-GA**

3

4   Marjan Salari[1], Mohammad Reza Nikoo[2*], Abdullah Al-Mamun[3], Gholam Reza Rakhshandehroo [4],

5   Mehrdad Ghorbani Mooselu[5]

6   **Abstract**

7   Antibiotics are considered among the most non-biodegradable environmental contaminants due to their

8   genetic resistance. Considering the importance of antibiotics removal, this study was aimed at multi-

9   objective modeling and optimization of the Fenton-like process, homogeneous at initial circumneutral pH.

10   Two main issues, including maximizing Ciprofloxacin (CIP) removal and minimizing sludge to iron ratio

11   (SIR), were modeled by comparing central composite design (CCD) based on Response Surface

12   Methodology (RSM) and hybrid Artificial Neural Network-Genetic Algorithm (ANN-GA). Results of

13   simultaneous optimization using ethylene diamine tetraacetic acid (EDTA) revealed that at pH$\cong$7, optimal

14   conditions for initial CIP concentration, Fe^{2+} concentration, $[H_2O_2]/[Fe^{2+}]$ molar ratio, initial EDTA

15   concentration, and reaction time were 14.9 mg/L, 9.2 mM, 3.2, 0.6 mM, and 25 min, respectively. Under

16   these optimal conditions, CIP removal and SIR were predicted at 85.2% and 2.24 (gr/M). In the next step,

17   multilayer perceptron (MLP) and radial basis function (RBF) artificial neural networks (ANN) were

18   developed to model CIP and SIR. It was concluded that ANN, especially multilayer perceptron (MLP-ANN)

19   has a decent performance in predicting response values. Additionally, multi-objective optimization of the

20   process was performed using Genetic Algorithm (GA) and Non-dominated Sorting Genetic Algorithm-II

21   (NSGA-II) to maximize CIP removal efficiencies while minimizing SIR. NSGA-II optimization algorithm

22   showed a reliable performance in the interaction between conflicting goals and yielded a better result than

[1] Assistant Professor, Department of Civil Engineering, Sirjan University of Technology, Sirjan, Iran.
[2] Associate Professor, Department of Civil and Architectural Engineering, Sultan Qaboos University, Muscat, Oman (Corresponding Author: m.reza@squ.edu.om).
[3] Associate Professor, Department of Civil and Architectural Engineering, Sultan Qaboos University, Muscat, Oman.
[4] Professor, Department of Civil and Environmental Engineering, Shiraz University, Shiraz, Iran.
[5] Ph.D. Research Fellow, Department of Engineering and Science, University of Agder, Norway.

the GA algorithm. Finally, TOPSIS method with equal weights of the criteria was applied to choose the best alternative on the Pareto optimal solutions of the NSGA-II. Comparing the optimal values obtained by the multi-objective response surface optimization models (RSM-CCD) with the NSGA-II algorithm showed that the optimal variables in both models were close and, according to the absolute relative error criterion, possessed almost the same performance in the prediction of variables.

Keywords: Pharmaceutical compounds, Ciprofloxacin antibiotic, Homogeneous processes, Multi-objective optimization.

Introduction

There is a growing tendency in medications usage, especially antibiotics. It is estimated that antibiotics production is about 100,000-200,000 tons per year (Bajpai et al., 2014). High consumption of antibiotics and release of their residuals cause environmental problems (Gagnon et al., 2008; Manyi-Loh et al., 2018), such as drug resistance in humans and also affects non-target pathogens, alters the structure of algae in water resources, and interferes with the plant's photosynthesis (Wei, 2011; Kovalakova et al., 2020). One of the famous families of antibiotics is fluoroquinolones. Ofloxacin (OFL), ciprofloxacin (CIP) and norfloxacin (NOR) are among the antibiotics of this family, widely used in therapeutic fields (Capriotti et al., 2012; Mayer and Takiff, 2014; Salari et al., 2021a; Rakhshandehroo et al., 2018). Since CIP (Molecular Weight 331.35 g/mol) is the most frequently detected worldwide, it was considered a model compound for antibiotic agents (Kümmerer, 2009; Lapworth et al., 2012; Li et al., 2018).

In the simple Fenton reaction, iron ions and hydrogen peroxide are the homogeneous catalysts, which play the key role in acidic conditions. The hydroxyl radicals are generated by a complex set of reactions during the Fenton process (Salari et al., 2018a, b, c; Torres-Pinto et al., 2020). The most significant variable in the Fenton reaction is the pH of the solution. It is believed that the optimum range of pH for this process is mainly approximately 3 (Mahamuni and Adewuyi et al., 2010). This is mainly because at pH values higher than 4, due to the ferric hydroxide precipitation, the performance of the Fenton process decreases. Under

49 these conditions, fewer free iron ions are catalytically available for decomposition, and as a result, fewer

50 hydroxyl radicals are produced. According to literature, the Fenton process's optimal conditions depend on

51 the maximum production of hydroxyl radicals (Neyens and Baeyens, 2003; He and Zhou et al., 2017).

52 Although the Fenton process is used in most industrial wastewater treatment plants, it has limitations, such

53 as pH conditions for the optimal solution, which is typically controlled by adding acid. However, adding

54 acid for pH adjustment (or pH less than 3) increases the operation costs (Usman et al., 2016). Several studies

55 investigated Fenton reaction defects, but a notable knowledge gap still exists on the effects of operational

56 parameters and the feasibility of using various chelating agents (organic ligands) on CIP oxidation during

57 the process. Chelating agents have been commonly used to achieve a stable amount of Fe (II) in the solution

58 (Zhou et al., 2013). Over the last two decades, nitrilotriacetic acid (NTA) and ethylene diamine tetraacetic

59 acid (EDTA) have been extensively applied as Fe (II) stabilizers (Miao et al., 2018). Therefore, in this study,

60 a comparison was made on CIP oxidation under different pHs using different concentrations of EDTA.

61 Notably, selecting the type of chelating agent has been based on library studies, ligand structure, commercial

62 availability, and economic concerns (Messele, 2014; Vicente et al., 2011). In this paper, Response Surface

63 Methodology (RSM) based on Central Composite Design (CCD) was employed to model and optimize two

64 main responses, namely, maximizing CIP removal and minimizing sludge to iron ratio (SIR) using EDTA.

65 Artificial Neural Network (ANN) is an effective tool for nonlinear multivariate modeling, capable of

66 learning the trend in historical data. Comparing ANN to RSM (i) ANN does not require previous

67 performance characteristic and (ii) ANN can approximate universally, meaning that almost all nonlinear

68 functions, including quadratic are approximated, while RSM can be applied just for quadratic

69 approximations (Desai et al., 2008). Various studies have suggested that an ANN basis requires a much

70 larger dataset (experiments) than RSM, however, if the dataset is statistically well distributed in the input

71 domain, ANN would suffice the design of experiments (DOE). Under such conditions, RSM data would be

72 sufficiently adequate to construct an ANN model. Previous studies have widely compared RSM and ANN

73 models by the same DOE and optimized the ANN model with a Genetic Algorithm (GA) (Desai et al.,

74 2008; Jacob and Banerjee, 2016; Talwar et al., 2019; Park et al., 2020; Ahmadi et al., 2021). GA has been

75 proven to be an ideal technique for solving various optimization problems in biochemical engineering

76 (Sarkar and Modak, 3003; Nandi et al., 2002). In direct methods, the multi-objective optimization issue was

77 solved in its original form, i.e., multi-objective. Non-dominated Sorting Genetic Algorithm-II (NSGA-II)

78 evolutionary algorithm has an excellent overall performance, and it is one of the most popular direct

79 methods for solving multi-objective optimization problems (Deb et al., 2002). The following are some

80 recent findings in this field. Vinayagam et al. (2022a) investigated the adsorption of hexavalent Chromium

81 using a sugar-consumed macroalgae biomass of Ulva prolifera. In this study, Chromium (VI) adsorption

82 from aqueous solutions was investigated under different conditions of pH, adsorbent amount, stirring speed,

83 and time to evaluate. Independent variables were optimized using a statistical method (RSM) and ANN tool

84 using experimental data. Under optimal conditions, the maximum adsorption was reported as $99.11\pm0.23\%$

85 using U.prolifera. Finally, comparing different parameters in RSM and ANN models showed that the ANN

86 model with a high coefficient (R^2_{ANN}: 0.9844, R^2_{RSM}: 0.9721) and low MSE (MSE_{ANN}: 3.7002, MSE_{RSM}:

87 6.2179) is more accurate in response prediction than the RSM model. Thus, the consumed biomass of

88 U.prolifera may be reliably used as a low-cost adsorbent for Chromium (VI) removal, and the adsorption

89 process may be modeled and predicted effectively using ANN. In addition, Vinayagam et al. (2022b)

90 synthesized magnetic activated charcoal/Fe_2O_3 nanocomposite (AC/Fe_2O_3NC) using spondias dulcis leaf

91 extract in an easy and fast method. Their results showed that the predictive ability of ANN (R^2= 0.99) was

92 better than the quadratic RSM model (R^2= 0.93). Therefore, this nanosorbent may be used as an excellent

93 alternative to 2,4-D removal from water bodies. Talwar et al. (2019) investigated the modeling of

94 metronidazole antibiotic removal using dual degradation of photo-Fenton and photocatalysis by composite

95 materials consisting of fuller soil and cast sand. The dual process facilitated a significant reduction in

96 treatment time because 80% of the combination was decomposed with 30 min of reaction. ANN model

97 coupled with GA was used to optimize input variables such as H_2O_2 dose, treatment time, number of grains,

98 pH, etc. The results showed that the maximum degradation was achieved in 120 min with an oxidant dose

99 of 1050 mg/L, pH 3.5, current intensity 25 W m^{-2} and A/V ratio 0.273 cm^2 mL^{-1}. The simultaneous effect

100   of two processes (80% decomposition in 30 min) until each process is applied separately was to reduce the

101   degradation time and increase the reaction rate constant. The results confirmed applying ANN coupled with

102   GA to optimize various parameters. Table 1 provides a summary of previous studies conducted in recent

103   years

104   Table 1. Summary of previous studies conducted in recent years

Treatment parameters	Contaminant	Main findings	References
Initial CEX concentration =15–55 (mg/L), Initial pH= 3–11, Electrolysis time= 20–40 (min), and Electrode type = Insulated and non-insulated)	Cephalexin Antibiotic	This study RSM-CCD, Artificial Neural Network (ANN) and Adaptive Neuro Fuzzy Inference System (ANFIS) were used to evaluated modeling and Optimizing removal of CEX antibiotics from Water. The results showed that the highest rate of CEX antibiotic removal by experimental data and predicted models were 88.21% and 93.87%, respectively. Based on the statistical indices were applied for assessment, ANFIS implemented better than ANN and RSM-CCD models.	(Arab et al., 2022)
Initial tetracycline concentration = 40–250 (mg/L), Concentration of H_2O_2= 20–600 (mg/L), and Concentration of Fe(II) = 0–60 (mg/L)	Tetracycline Antibiotic	Under optimal conditions hydrogen peroxide 310 (mg/l), Fe^{2+} 30 (mg/l), tetracycline 145 (mg/l), the highest (R^2= 100) efficiencies was 100%	(H Mahdi et al., 2021)
Contact time= 3.65 h, Number of beads= 98, Concentration of H_2O_2= 800 (mg/L).	Real industrial pharmaceutical effluent	This study, new composite granules was used as a surface for TiO_2 coating. Microbial experiments confirmed the effluent discharge according to disposable standards, and finally, a 75% reduction in COD was achieved in 5 hr.	(Talwar et al., 2021)

Water treatment residuals (WTR) concentration (g/L)= 10-30, Initial Dye concentration (mg/L)= 25-75, pH=3-5.	Dye removal (%)	The results of this study showed that under optimal conditions dye removal (%) was by CCD-RSM and ANN 52.0% and 52.2% , respectively. This study showed that optimization/prediction of the dye removal process is possible using the RSM-ANN approach.	(Gadekar et al., 2019)
Current intensity = 0.25–3 A, Reaction time= 10–90 (min), Concentration of $FeSO_4$ = 0.20–1.0 (mM).	Real textile wastewater	The optimal values of the parameters current, reaction time and concentration were $FeSO_4$ 0.32 A, 90 (min) and 0.53 (mM), respectively. The results indicated that the predicted parameters are well consistent with the experimental data.	(Kaur et al., 2019)
Concentration of TiO_2 $(g.L^{-1})$ = 0.4-2, pH= 3-11, Concentration of Ornidazole $(g.L^{-1})$= 0.01-0.03, Reaction time (min)= 30-180.	Ornidazole Antibiotic	Optimization and modeling of the ornidazole antibiotic were evaluated using TiO_2 as a photocatalyst and ANN. Under optimal conditions, the percentage of degradation using BBD, simulated with ANN and with experimental run were predicted to be 84.02, 82.63 and 77.7%, respectively. The results indicated that the predictions consistented with the experimental results.	(Talwar et al., 2018)

105

106 Due to the high and arbitrary use of antibiotics and the impossibility of eliminating such compounds with

107 common processes in a residential, hospital, or pharmaceutical wastewater treatment plant, investigating

108 effective and feasible methods is vital (Al Maadheed et al., 2018; Talwar et al., 2020; Salari et al., 2021b).

109 We analyzed and optimized the effects of environmental component concentrations, namely CIP (mg/L),

110 ferrous ions $[Fe^{2+}]$ (mM), $[H_2O_2]/[Fe^{2+}]$ mole ratio, and EDTA (mM) using the response level methodology.

111 Also, the application of a chelating agent to remove CIP antibiotics from aqueous media under neutral pH

112 conditions was investigated. The efficiency of predictive models presented by RSM-CCD and ANN-GA,

113 NSGA-II were evaluated. The optimal conditions presented by both methods have been experimentally

114 confirmed. The novelty of this work lies in the comparison of RSM-CCD, ANN-GA, and NSGA-II models

115 to enhance the Fenton-like process, homogeneous under neutral pH conditions, for CIP degradation.

116 **2. Material and Methods**

117 **2.1. Reagents**

118 Analytical grade chemicals were utilized without purification (Table S1).

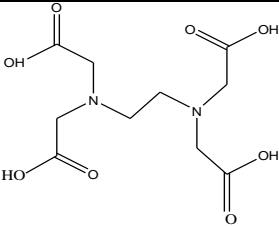119 **2.2. Using Chelating-Agent**

120 The use of chelating-agent in oxidation processes is a new and promising technology. In fact, the chelating-

121 agent is an organic compound with several rings and a high tendency to connect to a metallic element. The

122 most common metal ligands are oxygen, nitrogen, and sulfur atoms. Aminopolycarboxylic acids are one of

123 the most important groups of organic chelating agents, which have the ability to capture metal ions (Flora

124 and Pachauri, 2010). Ethylene Diamine Diacetic Acid (EDDA), Ethylene Diamine Tetra acetic Acid

125 (EDTA), Diethylene Triamine Pentaacetic Acid (DTPA), Imino Diacetic Acid (IDA), Hydroxyethyl

126 Ethylene Diamine Triacetic Acid (HEDTA), and Nitrilotriacetic acid (NTA) are example groups in this

127 family, while the latter has the most applications (Messele, 2014).

128 Based on the literature, chelating agents are broadly used, e.g., for metal ions' decomposition, inhibition of

129 metal-catalyst reaction, removal of metal ions, and increased metal availability. Also, it seems that by

130 adding chelating agents at pH = 6-7, stable chelates will be formed with iron ions, which makes these ions

131 available for reaction with hydrogen peroxide (H_2O_2), producing hydroxyl radicals, and partially preventing

132 the sequestration of iron ions (Messele, 2014). EDTA organic chelates (Table 2) has a high affinity for

133 heavy metal ions, especially iron, generating highly stable complexes. It is also found economically

134 affordable and abundantly available (Messele, 2014).

135 **Table 2.** Chemical formula and structure EDTA (Adopted from Messele, 2014)

Composition name	Molecular weight	Molecular formula	Molecular structure
Ethylene diamine tetra acetic acid (EDTA)	292.24 (gr/mol)	$C_{10}H_{16}N_2O_8$	

136

2.3. Predictive modeling and optimization methods

2.3.1. Experimental design

When many parameters and relationships affect the response variable, RSM methodology designs the experiments effectively, and computes the optimal values of several variables simultaneously utilizing minimal quantitative data, and resources (Ehteshami et al., 2021; Mahmoudpour et al., 2021). Common subset methods for RSM design include CCD and BBD. A comparison of CCD and BBD experimental design methods is given in Table S2. Normally, CCD has more features than BBD, but selecting an appropriate design depends upon the nature of parameters and preliminary information about them. Based on the explanations provided in Table S2 and considering the number and conditions of independent variables in our study, CCD method has been selected which has rotation capability and widespread use in various studies. The CCD can fit a second-order model, and has the necessary features for response level designs (Shoorangiz et al., 2019; Salari et al., 2021b; Mahmoudpour et al., 2021; Salari 2022).

Table S3 shows the number of selected levels of Fenton-like homogenous organic decomposition process using the chelating agent when all experiments are performed at pH$\cong$7. The effective variables and selected levels for the effective parameters in the experimental design were presented in Table S4, with six repetitions of the central points, as shown in Table S5. In the CCD design method, the number of required experiments (N) was defined as $N=n_0+2K+2^K$, in which K and n_0 are the number of input variables and the number of central points, respectively.

8

155   Also, each parameter is divided into five different levels $(+\propto, +1, 0, -1, -\propto)$, where α is the axial point

156   and its value depends on the number of input variables (Ngan et al., 2014; Rakić et al., 2014). However,

157   the operating range of the experiments for the independent parameter was determined based on a literature

158   review and the results of initial experiments, such as one factor at a time.

159   **2.3.2. Artificial neural network (ANN)**

160   ANN model involves 1- data generation, 2- data processing, 3- the network structural design, 4- selection

161   of the training algorithm, 5- network training, and 6- testing the trained network (Yamashita et al., 2018).

162   Although several network structures exist for modeling, the most popular ANN structures include

163   multilayer perceptron (MLP) and radial-based functions (RBF) (Ahari et al., 2013).

164   Multi-layer perceptron artificial neural network were developed with radial base function taking into

165   account input factors i.e., initial concentration of CIP (mg/l), iron ion concentration (mM) $[Fe^{+2}]$, molar

166   ratio $[H_2O_2]/[Fe^{+2}]$ and concentration of EDTA (mM). We used Matlab® R2015a for the objectives

167   prediction. The ANN was developed based on the results of 21 experiments, and validated by the results of

168   9 experiments.

169

170   **2.3.2.1. Multilayer perceptron neural network (MLP)**

171   Four models of feed-behind neural networks with three layers (i.e., input, hidden, and output) and various

172   transmission functions were developed to assign the best transmission functions in the hidden and output

173   layers. Initially, the cross-validation method was used to obtain the best network design and solve the

174   problem of data scarcity. After selecting the best models, multi-objective optimization of the process was

175   performed by two methods, simple GA and NSGA-II.

176   Data obtained during the experiments were introduced to the network in the form of a 4×30 matrix for the

177   input and a 1×30 matrix for the output. The data was divided 70%, 20%, 10% into training, testing and

178   validation sets, respectively. The input layer had 4 neurons, equal to the number of input variables, which

9

179   was optimized after specifying the best network from the four mentioned models. The number of output

180   parameters directly affects the number of neurons in the output layer. In ANN model, Levenberg-

181   Marquardt backpropagation (LMBP) was used for network training, and the output was compared with the

182   expected output. In this type of neural network, investigating the relative importance of each input variable

183   on the output response can be estimated from Garson's equation according to equation 1:

$$I_j = \frac{\sum\limits_{k=1}^{k=N_i}\left(\dfrac{\sum\limits_{m=1}^{m=N_h}\left|W_{jm}{}^{g}\right|}{\left|W_{km}^{ih}\right| \times W_{mn}^{ho}}\right)}{\sum\limits_{k=1}^{k=N_i}\left(\dfrac{\sum\limits_{m=1}^{m=N_h}\left|W_{km}^{ih}\right|}{\sum\limits_{k=1}^{k-N_i}\left|W_{km}^{ih}\right| \times W_{mn}^{ho}}\right)} \tag{1}$$

184   Where, N_i, N_h are the number of neurons in input and hidden layers, I_j shows the relative significance of

185   jth input variable on the output variable, and W is connection weight. The superscripts 'i', 'h' and 'o'

186   demonstrate input, hidden, and output layers, while subscripts 'k', 'm' and 'n' illustrate input, hidden, and

187   output neurons, respectively (Elmolla et al., 2010; Aleboyeh et al., 2008).

188

189   **2.3.2.2. Radial basis function (RBF)**

190   In the radial basis function artificial neural network (RBF-ANN), newrb function was used to adjust the

191   input data. Theoretically, RBF network (like its MLP counterpart) can perform any kind of continuous

192   nonlinear mapping between inputs and outputs. While MLP networks have public activity functions, the

193   activation functions are local to these networks. The number of neurons in the hidden layer was obtained

194   by sensitivity analysis, and neurons in the output layer were equal to the number of outputs. For training, it

195   is necessary to adjust the activity center together with the weights. Weights and the activity function center

196   were adjusted by the descending gradient method according to the least sum of squared errors (Al-Shamisi

10

197   et al., 2014), and the optimal artificial neural network was selected based on the least mean squares error

198   (MSE) and the correlation coefficient (R^2).

199   **2.3.2.3. Performance of models**

200   Evaluation of neural network performance has been done through some statistical indicators such as MSE,

201   root mean square error (RMSE), R^2, and mean absolute relative error (MARE) according to equations 2 to

202   4:

$$MSE = \sum_{i=1}^{n} (y_{Obs,i} - y_{model,i})^2 / n \qquad (2)$$

$$RMSE = ((\frac{1}{n} \sum_{i=1}^{n} (y_{obs,i} - y_{model,i})^2)^2)^{1/2} \qquad (3)$$

$$R^2 = \frac{(\sum_{i=1}^{n} (y_{obss,i} - y_{obs,.mean})(y_{model,i} - y_{model.mean})^2}{\sum_{i=1}^{n} (y_{obs,i} - y_{obs,mean})^2 (y_{model,i} - y_{model,mean})^2} \qquad (4)$$

203

204   Where, *n*, y_{Obs} and $y_{mod\,ls}$ are the number of data, measured and the modeled outputs, respectively. $y_{Obs,Mean}$

205   and $y_{Model,Mean}$ are the average experimental measured values and the average values of model predictions

206   (Elmolla et al., 2010; Aleboyeh et al., 2008; Shanmugaprakash and Sivakumar, 2013).

207

208   **2.3.3. Genetic Algorithm (GA)**

209   A genetic algorithm is a subset of evolutionary computational algorithms that is directly related to artificial

210   intelligence and uses biological concepts such as inheritance, mutation, sudden selection, natural selection,

211   and composition. It is often necessary to optimize an objective in relation to several (sometimes) conflicting

212   goals. There are two general solutions for multi-objective optimization problems 1) decomposition

213   methods, and 2) direct solution methods (Fan et al., 2017).

214   In decomposition methods, a multi-objective optimization problem is first transferred to a single-objective

215   one. The simplest and the most practical analysis approach is then assigning weights to targets (Coello,

216   2007), whereby a weight is assigned to each goal based on its importance. Finally, multiplying this weight

217   by the value of each goal, a simple and solvable goal function is defined for the optimization problem. In

218   other words, rather than minimizing a number of different objective functions ($min\ f_i(x),\ i = 1,2,..,n$)

219   the following equation is minimized (Yang and Moodie, 2011):

$$\min f_{wi}(x) = \min \sum_{i=1}^{n} w_i\ f_i(x) \tag{5}$$

220   In the decomposition methods, conversion of a multi-objective problem to a single-objective one causes

221   loss of some information in the decision space. To overcome this problem, the problem must be solved

222   several times, which is time-consuming and generates a different answer each time.

223   One of the advantages of direct methods is fast and accurate operation speed (Yang and Moodie, 2011). In

224   the NSGA-II method, population members are organized (sorted) according to the non-dominance concept.

225   The purpose of implementing NSGA-II and GA are to achieve an interaction curve reflecting costs and

226   benefits (Cámara et al., 2012; Deb et al., 2002; Mooselu et al., 2020). In this process, the goal is to find a

227   set of answers that minimizes or maximizes the objective function, while several conflicting goals are

228   optimized. At this stage, the best ANN models chosen at the previous stage were connected to GA and

229   NSGA-II algorithms as a fitting function, and the multi-objective optimization process was performed with

230   GA according to the following formulations:

231   *Design variables: Fe^{2+} concentration, $[H_2O_2]/[\ Fe^{2+}]$ Mole ratio, EDTA concentration*

$$\text{Minimize} - (w_1 f_1(\vec{x})_n - w_2 f_2(\vec{x})_n) \tag{6}$$

232   *Subject to*:

$$5\ mM < Fe^{2+}\ \text{Concentration} < 21\ mM \tag{7}$$

$$2 < [H_2O_2]\ /[\ Fe^{2+}]\ \text{Mole ratio} < 4 \tag{8}$$

12

$$0 < \text{EDTA Concentration} < 2 \ \text{mM} \tag{9}$$

233   In equation 6, w_i is the weight of each target (response) with the normalized value of $f_i(x)_n$. Indices 1 and 2

234   reflect CIP removal and SIR reduction, respectively. As mentioned, solving a multi-objective optimization

235   problem by a single-objective method eliminates part of the decision space and does not reveal all possible

236   optimal solutions. The main advantage of NSGA-II evolutionary optimization algorithm is its ability to

237   consider selected responses simultaneously (Deb et al., 2002). The formulation of NSGA-II direct multi-

238   objective optimization algorithm with two objectives was defined as the following equations:

239   *Design variables: Fe^{2+} concentration, $[H_2O_2] / [Fe^{2+}]$ Mole ratio, EDTA concentration*
240

$$\text{Maximize } f_1(\vec{x}) \tag{10}$$

$$\text{Minimize } f_2(\vec{x}) \tag{11}$$

241   *Subject to:*

$$5 \ \text{mM} < Fe^{2+} \ \text{Concentration} < 21 \ \text{mM} \tag{12}$$

$$2 < [H_2O_2]/[Fe^{2+}] \ \text{Mole ratio} < 4 \tag{13}$$

$$0 < \text{EDTA Concentration} < 2 \ \text{mM} \tag{14}$$

242

243   In order to obtain optimal general answers, the population of each generation was considered to be 120, of

244   which 35% were in the first unfavorable front. Upon reaching the maximum generation condition (100

245   generations), the final unsuccessful front was obtained in the form of an interaction curve. Then, the

246   TOPSIS multi-criteria decision-making model was applied to choose the best option among the optimal

247   solutions (42 answers).

248   **3. Results and Discussion**

249   In this section, changes in CIP antibiotic concentration and SIR were measured at specified time intervals

250   (25 minutes) considering input variables of ciprofloxacin initial concentration (mg/L), iron ion

251   concentration $[Fe^{2+}]$ (mM), molar ratio $[H_2O_2]/[Fe^{2+}]$), EDTA concentration (mM) and PH$\cong$ 7. Results are

252   presented in Table 3.

253   **Table 3.** Results obtained based on experimental runs and predicted by (RSM-CCD)

Run's Number	Response 1 CIP removal (%)	Response 2 SIR (gr/M)
1	73.00	2.81
2	62.00	3.65
3	90.00	3.60
4	53.00	3.30
5	87.91	3.56
6	80.00	3.62
7	68.00	4.09
8	94.00	3.20
9	83.00	3.18
10	47.00	3.45
11	38.00	4.85
12	79.00	3.36
13	56.00	3.54
14	93.00	3.87
15	87.00	3.40
16	83.00	2.68
17	74.30	2.71
18	53.00	3.02
19	87.91	3.33
20	84.60	2.43
21	65.34	4.23
22	95.00	3.56
23	70.27	3.01
24	78.52	2.24
25	83.00	3.40
26	73.00	4.20
27	87.91	3.56
28	75.97	3.84
29	84.32	3.45
30	58.00	4.09

254

255 Based on the results and statistical analysis performed on the objectives, the application of a quadratic

256 statistical model was evaluated based on an appropriate experimental design. The final model was obtained

257 for the two responses (CIP removal and SIR reduction) as a function of effective coded variables according

258 to the following equations:

259 **CIP removal (%)**

260 $$Y_1 = +90.29 - 4.52\,A + 1.91\,B + 1.87C - 8.75\,D - 2.13\,A^2 - 4.04\,B^2 - 2.24\,C^2 - 0.91\,D^2 \quad (15)$$

261 **SIR reduction (gr/M)**

262 $$Y_2 = +3.81 + 0.084\,B + 0.40\,D - 0.28\,BD - 0.19\,A^2 - 0.22\,B^2 - 0.099\,C^2 + 0.080\,D^2 \quad (16)$$

263   In equations (15) and (16), a positive (negative) sign, reflects a direct (inverse) effect of variables on the

264   target. These equations also illustrate the magnitude of parameters' effect on the target surface and their

265   interactions with the target relative to one another. Results for the analysis of variance performed on the

266   models (CIP removal and SIR reduction) for their validation are presented in Table 4. P-values < 0.05

267   indicate the model variables are appropriate, and p-value values>0.1 indicate that such variables are

268   inappropriate.

269   **Table 4.** Results for model accuracy based on analysis of variance (ANOVA)

270   **a) CIP removal (%)**

Source	Sum of squares	Degree of Freedom	Mean square	F value	P-value Prob > F	
Model	5943.60	8	742.95	28.46	< 0.0001	**significant**
A-Initial CIP (mg/L)	491.23	1	491.23	18.82	0.0003	
B- Fe^{2+} (mM)	87.63	1	87.63	3.36	0.0811	
C-H_2O_2/Fe^{2+}	84.08	1	84.08	3.22	0.0871	
D-EDTA (mM)	1838.90	1	1838.90	70.45	< 0.0001	
A^2	123.91	1	123.91	4.75	0.0409	
B^2	447.22	1	447.22	17.13	0.0005	
C^2	138.14	1	138.14	5.29	0.0318	
Residual	548.12	21	26.10			
Lack of Fit	501.51	16	31.34	3.36	0.0927	**not significant**
Pure Error	46.61	5	9.32			

271   Std Dev = 5.11   CV% = 6.83   PRESS= 1595.39 R^2= 0.91 Adj. R^2= 0.88   Adequate Precisions= 22.04

272

273

274

275

276

277   **b) SIR reduction**

Source	Sum of squares	Degree of freedom	Mean square	F value	P-value Prob > F	
Model	7.85	7	1.12	19.71	< 0.0001	**significant**
B-Fe^{2+} (mM)	0.17	1	0.17	2.96	0.0995	
D-Initial EDTA (mM)	3.80	1	3.80	66.78	< 0.0001	
BD	1.27	1	1.27	22.34	0.0001	
A^2	1.02	1	1.02	17.84	0.0003	
B^2	1.28	1	1.28	22.52	< 0.0001	
C^2	0.27	1	0.27	4.69	0.0414	
Residual	1.25	22	0.057			
Lack of Fit	0.78	17	0.046	0.49	0.8762	**not significant**
Pure Error	0.47	5	0.094			

278   Std Dev =0.24 CV% = 6.87 PRESS= 2.42 R^2= 0.86 Adj. R^2= 0.81   Adequate Precisions = 18.72

279 As shown in Tables 3 (a) and (b), and according to the rationale offered by the statistical analysis, obtained

280 model results are satisfactory and logical. Since AP values for the two targets (CIP removal and SIR

281 reduction) are both above 4, 22.04 and 18.72, respectively, therefore, it may be concluded that the results

282 are satisfactory. Figure 1 (a-b) shows the scatter plot of experimentally measured values versus the values

283 predicted by the models. As shown, there is a reasonable interconnection between the two rationalizing the

284 results being logical.

285
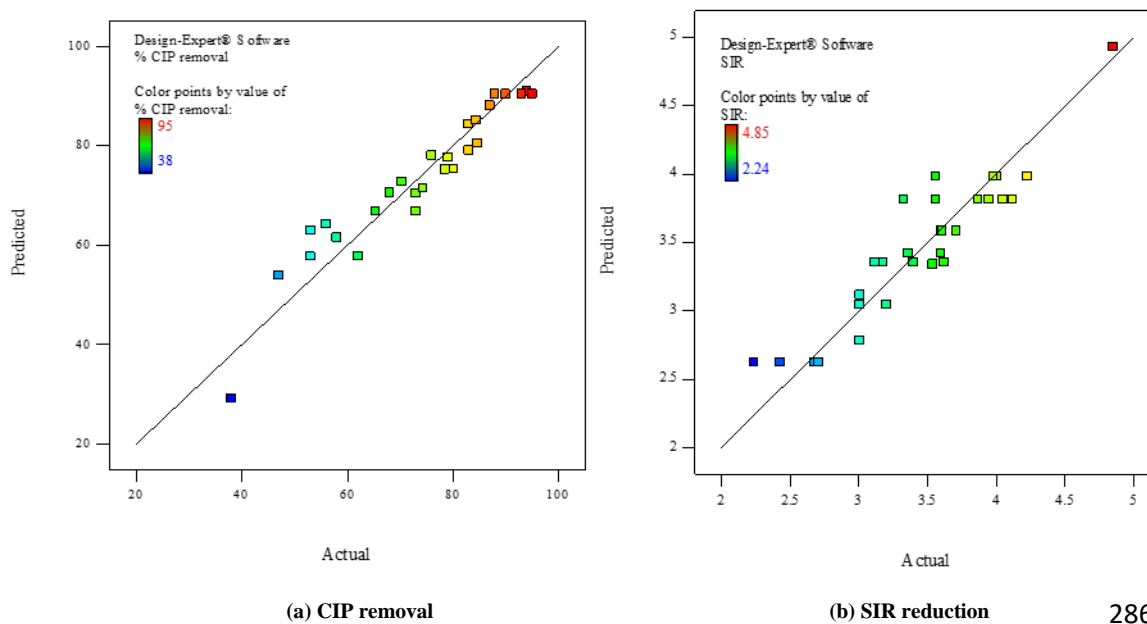
(a) CIP removal   (b) SIR reduction   286

287 **Figure 1.** Measured values versus predicted values a) CIP removal percentage and b) SIR reduction

288

289 Once the models' accuracy was ensured, a perturbation plot for each target was drawn to measure the

290 independent parameters' effect on each target and investigated separately (Figure S1). A positive effect of

291 an independent variable on the intended response means that as the variable increases, so does the response,

292 and to the contrary, a negative effect of the variable happens when an increase in the variable reduces the

293 response rate. In Figure S1-a, a relatively high curvature with positive effects on variables B (Fe^{2+}) and C

294 ($[H_2O_2]/[Fe^{2+}]$) was observed, while variables A (CIP Concentration) and D (EDTA Concentration) impose

295 negative effects on CIP removal response.

16

296   As observed, with increasing EDTA concentration from 0 to 1mM, the CIP decomposition rate increases

297   from 56% to 95%. This shows a positive effect of EDTA concentration on CIP decomposition. It has also

298   been reported in previous studies that Fe^{2+} ions released from minerals with chelating agents leads to an

299   increase in the homogenous Fenton-like reaction, apparently by weakening metal-oxygen bonds on the

300   surface of minerals in contact with the chelating agents (Sun et al., 2014; Matta et al., 2008). In addition, at

301   a pH of about (6.5-7), the EDTA complex apparently completes the Fenton reaction, and causes high

302   dissolution of Fe^{2+} ions in the solution, inhibiting sequestration of these ions (Diao et al., 2017).

303   In this study, the pollutant decomposition rate decrease from 95% to about 38% associated with EDTA

304   concentration increase from 1 to 2 mM was observed as a significant negative effect. The relatively high

305   EDTA concentration may explain the reason for consuming a large rate of hydroxyl radical (OH^0) produced

306   in the process. Other studies have suggested that an increase in EDTA concentration above a permissible

307   level is known as a hydroxyl radical (OH^0) consumer; a process that reduces the speed of the Fenton reaction

308   (Diaoa et al., 2017). Results reveal that soluble Fe^{2+} ion concentration is maximized in the process at an

309   EDTA concentration of 1 mM, and at concentrations above 1 mM, a significant decrease would occur.

310   Under these conditions, Fe^{3+} ion concentration in the solution has an increasing trend. Notably, the EDTA

311   concentrations >1 mM inhibit CIP oxidation. Therefore, catalytic behavior is not enhanced by excessive

312   EDTA, rather, a high concentration of EDTA may inhibit hydroxyl radicals formation. Based on the

313   literature, the ligand to metal ratio is very important because the production of radicals decreases in the

314   presence of excess ligand (Messele, 2014; Diaoa et al., 2017).

315   In the next step, single-objective optimization was performed using the response surface method. Thus, a

316   maximum CIP removal of 95% was predicted when keeping the variables in the design range with the initial

317   CIP concentration, [Fe^{2+}] ion concentration, [H_2O_2]/[Fe^{2+}] molar ratio, and EDTA concentration variables

318   as 29.1 mg/L,13.9 mM, 2.7 and 0.81 mM, respectively.

319   SIR production in Fig. S1-b depicted a relatively high curvature with a positive effect on variable D (EDTA)

320   and a negative effect on other variables at the corresponding response. As mentioned, the pollutant

321   decomposition rate decreases with increasing EDTA concentration from 1 mM to 2 mM. It is mainly

322   because the number of hydroxyl radicals produced by the Fenton process decreases at relatively high EDTA

323   concentrations. Apparently as EDTA concentration increases, a large number of radicals are consumed to

324   destroy EDTA rather than being used for CIP decomposition. Meanwhile, Fe^{2+} concentration in the medium

325   is maximized at a certain EDTA concentration (1 mM). However, a significant reduction in the ion's

326   concentration occurs in the range of 1-2 mM EDTA. On the other hand, under the same conditions, Fe^{3+}

327   concentration increases with rising EDTA in the medium. A similar study by Daya et al. (2017) reported

328   similar behavior for the independent variables.

329   In summary, it may be concluded that certain concentrations may be used for these organic complexes so

330   that the modified Fenton reaction might be applied directly to the environmental effluents at a neutral or

331   slightly alkaline pH. Under the single-objective optimization conditions using a response surface

332   methodology, the maximum SIR reduction was equal to 2.21 gr/M if the variables were kept in the design

333   range. Also, optimal values for initial CIP concentration, $[Fe^{2+}]$ ion concentration, $[H_2O_2]/[Fe^{2+}]$ molar ratio,

334   and EDTA concentration were predicted as 38.16 mg/L, 5.32 mM, 2.21 and 0.56 mM, respectively.

335   Regarding the interaction of independent variables on the responses, no interaction was observed among

336   the variables in CIP removal model (according to equation 15). However, regarding the SIR model (based

337   on equation 16), the response surface plot of the interaction between the two influential variables of EDTA

338   and Fe^{2+} concentrations on the response was investigated simultaneously, while other variables were kept

339   constant at the center point (Figure 2).

Design-Expert® Software
Factor Coding: Actual
SIR (gr/M)
● Design points above predicted value
○ Design points below predicted value

4.85

2.24

X1 = B: Fe (mMl)
X2 = D: EDTA

Actual Factors
A: CIP (mg/l) = 56.00
C: H2O2/Fe2+ = 2.50

340
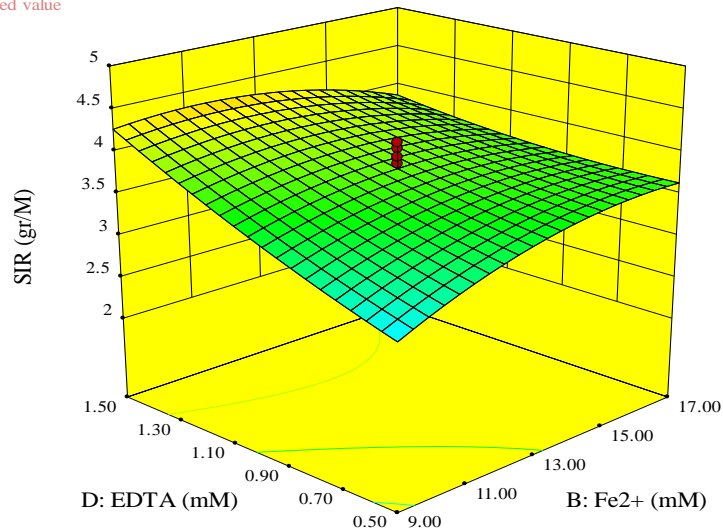
Figure 2. Response surface plot for SIR response as a function of Fe^{2+} and EDTA concentrations (mM) ($\frac{H_2O_2}{Fe^{2+}} = 3$,

Initial CIP= 56 mg/L)

As shown in Figure 2, increasing EDTA concentration had a positive effect on sludge production. For example, the sludge production efficiency reaches a maximum of 4.3 (gr/M) with an initial Fe^{2+} and EDTA concentrations of 9 mM and 1.5 mM, respectively. In contrast, if the initial Fe^{2+} concentration is equal to 17 mM, with EDTA concentration decrease from 1.5 mM to 0.5 mM, sludge production decreases to the rate of 2.71 mM. Furthermore, sludge production decreases with increasing iron concentration from 9 mM to 17 mM and decreasing EDTA concentration. In other words, to reduce sludge production efficiently, a simultaneous increase in iron and decrease in EDTA concentrations must be considered. Finally, the results of analysis of variance (ANOVA) indicated that all independent variables are effective on CIP removal response, but the initial CIP and EDTA con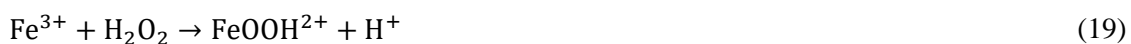centrations are the most influential ones. Furthermore, EDTA and Fe^{2+} concentrations are the most important independent variables affecting sludge production.

3.1. Multi-objective optimization by RSM-CCD and confirmatory experiments

19

354   Through a set of reactions presented by Haber and Weiss (Eqs. 17-23), the pollutant decomposition and

355   removal mechanisms may be followed by production of hydroxide radicals (Haber and Weiss, 1934;

356   Messele et al., 2019). As the radicals are released, they attack organic compounds and eventually, hydrogen

357   peroxide is converted to water and molecular oxygen (Messele et al., 2019). In the next step, if Fe^{3+} is

358   removed, then Fe^{2+} is gradually released and the reaction stops. Therefore, the main role of EDTA is to

359   retain Fe^{3+} in the solution without negatively affecting next steps, even at neutral pH (Messele et al., 2019).

360   Results indicated that addition of EDTA to the Fenton system actually led to more efficient use of H_2O_2,

361   causing an increase in iron-catalyzed H_2O_2 decomposition to radicals, thereby improving the contaminants

362   removal, similar to reports by other researchers. This may be considered as a solution to the problems of

363   traditional Fenton systems."

$$Fe^{2+} + H_2O_2 \rightarrow Fe^{3+} + HO^0 + OH^- \tag{17}$$

$$Fe^{2+} + HO^0 \rightarrow Fe^{3+} + OH^- \tag{18}$$

$$Fe^{3+} + H_2O_2 \rightarrow FeOOH^{2+} + H^+ \tag{19}$$

$$FeOOH^{2+} \rightarrow Fe^{2+} + HO_2^0 \tag{20}$$

$$Fe^{2+} + HO_2^0 \rightarrow Fe^{3+} + HO_2^- \tag{21}$$

$$Fe^{3+} + HO_2^0 \rightarrow Fe^{2+} + O_2 + H^+ \tag{22}$$

$$HO^0 + H_2O_2 \rightarrow H_2O + HO_2^0 \tag{23}$$

364   Numerous optimal points with high utilities were reported by Design Expert® software for a Homogeneous

365   Fenton-like process with a chelating agent. Based on the optimization model results, the values for initial

366   CIP concentration, Fe^{2+} concentration, the molar ratio $[H_2O_2]/[Fe^{2+}]$, EDTA concentration, and reaction

367   time were 14.90 mg/L, 9.20 mM, 3.2, 0.62 mM and 25 minutes, respectively. As shown in Table S5,

368   predicted models are in close agreement with observational values with an absolute relative error of less

369   than 5%.

370   **3.2. Initial pH effect in the absence and presence of EDTA**

371 Before numerical modeling, the role of EDTA was investigated by measuring independent variables under

372 optimal experimental conditions at different pHs and times to ensure the accuracy of obtained results

373 (Figure S2). Results showed that the lowest CIP degradation was observed in the homogenous Fenton

374 process at the absence of EDTA and a pH of 6.5. Similar results have been reported in the Fenton process

375 by previous researchers (Elmolla and Chaudhuri, 2009; Salari et al., 2018a; Rakhshandehroo et al., 2018;

376 Shorangize et al., 2019). To consider the bond between Fe and EDTA ions, effects of different pHs on the

377 Fenton oxidation process were investigated in the presence of EDTA (Figure S3).

378 As observed, the addition of EDTA did not improve the contaminant decomposition under pH~3.5

379 significantly. It is apparently because there are too many active Fe^{2+} ions in the soluble medium at pH~3.5,

380 and it is impossible to form Fe^{3+} as an insoluble precipitate. Therefore, EDTA presence does not change

381 the classical Fenton process conditions at pH~3.5. However, at pH 6.5 to 7, where sequestration of Fe^{3+}

382 occurs in the form of hydroxide ($Fe(OH)_3$), EDTA addition plays a significant role. It seems that through

383 stable chelates formation with iron ions (adding chelating agents at pH 6.5-7), these ions react with

384 hydrogen peroxide, preventing the sequestration of iron ions and producing hydroxyl radicals.

385 At pH≈8 with or without EDTA, the CIP decomposition rate is lower than that at other pH values. This is

386 mainly because in these conditions, increasing EDTA will not affect the rate of H_2O_2 decomposition, which

387 means H_2O_2 does not enter into the Fenton reaction for producing the hydroxyl radical (Szpyrkowicz et al.,

388 2001). An increase in pH higher than the neutral values decomposes hydrogen peroxide into water and

389 oxygen and delays the Fenton process. Such results are similar to studies by other researchers (Messele,

390 2014). As a result, the most important problem in the classical Fenton process (sludge production and

391 optimal performance at pH≤3) may be partially solved by increasing a certain rate of the chelating agents

392 (Li et al., 2015). The concentration of the chelating agent used and the initial pH of the solution are two

393 important factors in the successful execution of the process. This point reduces the major costs by

394 eliminating the need for primary acidification. Hence, it was concluded that the main EDTA role is its Fe^{3+}

395 retention in the neutral solution to stop affecting the rest of the steps. The positive effect of a Fenton reaction

396   in a low pH (3-4) range is, in many cases, to remove various types of contaminants. On the other hand,

397   there are reports that complex forms of iron work to decompose hydrogen peroxide in a much wider pH

398   range. Our findings are consistent with the related studies (Messele et al., 2019; Lee and Sedlak, 2009).

399   **3.3. Hybrid multi-objective optimization ANN-GA and ANN- NSGA-II**

400   **3.3.1. Predictive modeling with ANN-MLP and ANN-RBF**

401   Input variables in the ANN modeling are initial CIP concentration (mg/L), Fe^{2+} concentration (mM), the

402   molar ratio $[H_2O_2]/[Fe^{2+}]$, and EDTA concentration (mM) over a 25-min period. To construct the

403   perceptron neural network and determine the most suitable transmission functions in the hidden and output

404   layers for prediction of CIP removal and SIR reduction, four feed neural network models each having three

405   input, hidden and output layers were developed. Initially, the cross-validation method was used to obtain

406   the best network architecture and to solve the problem of low data numbers. According to the first part of

407   the research, after selecting the best models, multi-objective optimization of the process was performed by

408   two methods: Simple GA and NSGA II. One of the most basic parts of a neural network design is to

409   determine the transmission functions and number of neurons in the hidden and output layers. First, the

410   transmission functions were determined with 10 neurons in the hidden layer, and then, the number of

411   neurons in the hidden layer was optimized. For this purpose, four models of purelin-purelin, purelin-tansig,

412   tansig-purellin, and tansig-tansig were used as transfer functions in the hidden layer. The appropriate

413   criterion for determining the best transfer function was having the lowest MSE and the highest R^2. MSE

414   and R^2 values developed for two purposes (CIP removal and SIR reduction) may be seen in Figure S4 for

415   all four models. As shown, sigmoid tangent and linear transfer functions in the hidden and output layers

416   had the lowest MSE ($MSE_{CIP} = 5.1$, $MSE_{SIR} = 0.063$) and the highest R^2 ($R^2_{CIP} = 0.98$, $R^2_{SIR} = 0.98$),

417   respectively.

418   In the next step, neural networks with the mentioned architecture were created having different number of

419   neurons (from 1 to 20) in the hidden layer, and the optimal number of neurons was determined based on

420   the lowest MSE and the highest R^2, according to Figure S5. Finally, for the designed neural network model,

22

421 the optimal number of neurons for CIP removal was obtained with 7 and SIR with 10 neurons in the hidden

422 layer. It should be noted that increasing the number of neurons does not always improve network function,

423 but its should be proportional to the amount of data entering the neural network. Finally, the training results

424 for ANN-MLP and ANN-RBF models considering the minimum MSE and the highest R^2 for the two

425 objectives of CIP removal and SIR are shown in Tables S7 and S8. Using Garson's relation, the relative

426 importance of variables in predicting each target is presented in Figure 3.

427
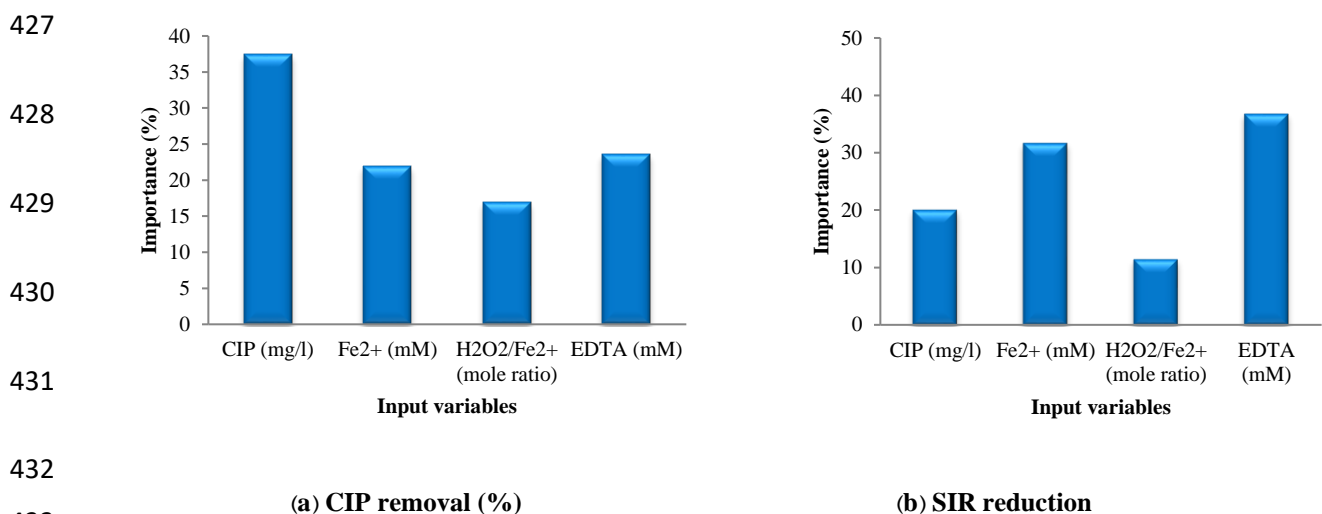
433 (a) CIP removal (%)   (b) SIR reduction

434 **Figure 3.** Relative importance of studied variables in predicting goals with Garson's equation

435 According to Figure 3, the most important variables for CIP removal, are initial CIP and EDTA

436 concentrations. Such variables for sludge production are EDTA and Fe^{2+} concentrations, respectively.

437 **3.3.2. Comparing the performance of RSM-CCD with ANN-MLP and ANN-RBF models**

438 In the next step, a series of analysis were performed on the network's response and experimental models of

439 the response surface. In this regard, all evaluated data were inputted to a network, and linear regression was

440 applied to the network output and the target vector (experimental results). Summary of performance

441 evaluation results for ANN-MLP, ANN-RBF, and RSM-CCD models based on MARE, MSE, and R^2 are

442 presented in Table 5.

443 **Table 5.** Summary of performance comparison for ANN-MLP, ANN-RBF and RSM-CCD models

Responses	Model	MARE (%)	MSE	R^2	Influential variables
CIP (%)	**ANN-MLP**	**0.91**	**2.36**	**0.98**	Initial CIP Concentration, EDTA Concentration
	ANN-RBF	9.73	67.15	0.84	
	RSM-CCD	5.59	7.10	0.92	Initial Concentration CIP, Concentration EDTA
SIR	**ANN-MLP**	**1.07**	**0.01**	**0.97**	EDTA Concentration, Fe^{2+} Concentration
	ANN-RBF	13.51	3.8	0.82	
	RSM-CCD	4.87	0.37	0.86	EDTA Concentration , Fe^{2+} Concentration

444

445   As shown in Table 5, ANN-MLP network performed better than ANN-RBF and experimental data model

446   (RSM-CCD) for both objectives (CIP removal and SIR). This proves high ANN-MLP capability in Fenton

447   process modeling.

448   Effective variables for the models output are also presented in the last column of Table 5. These are

449   identified based on Garson's equation and analysis of variance. The table reveals that effective variables in

450   CIP removal and SIR sludge production were similarly reported in both multilayer perceptron neural

451   network output models and the experimental designs. Finally, the best architecture of ANN-MLP was

452   linked with GA and NSGA-II algorithms to develop a hybrid multi-objective optimization model.

453   Comparison between experimental values and predicted ones using the ANN-MLP method are presented

454   in Figure S6. Similar results have been reported in the literature when comparing RSM-CCD and ANN

455   modeling results for other contaminants (Speck et al., 2016; Vinyagam et al., 2022a; Vinayagam et al.,

456   2022b).

457

458

459

460

### 3.3.3. Hybrid Multi-Objective Optimization by ANN-GA and NSGA-II

The purpose of using GA for optimization is to maximize CIP removal and minimize SIR. In order to optimize the multi-objective process with a single-objective genetic algorithm, a fitting function was defined for a weighted sum of the objectives, according to equations 6 to 9. Since the GA is a minimization algorithm, its target was entered into the fitting function with a negative sign to maximize the CIP removal. The weights of the two main targets, i.e., CIP removal rate and SIR were considered equal to 0.5. A maximum of 100 generations was considered as the condition for completion of the algorithm, which is shown in Figure 4.
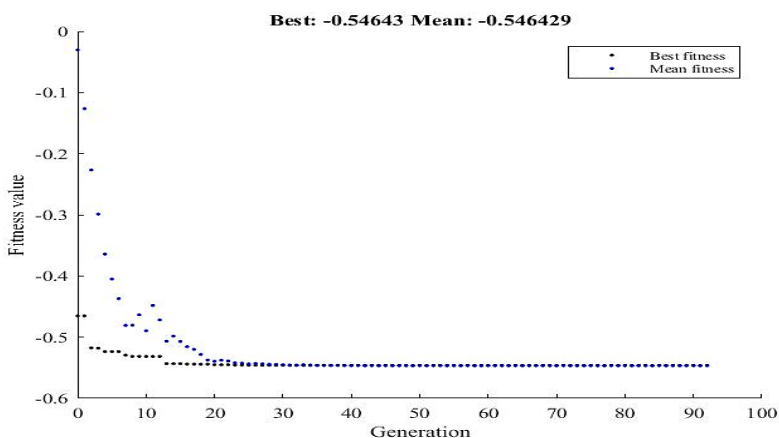
Figure 4. Convergence of a single-objective genetic algorithm to an optimal multi-objective solution

In this figure, the output fitness value is a defined fitting function, and the genetic algorithm objective is to minimize this value. According to the optimum response obtained by this method, Fe^{2+} concentration, H_2O_2/Fe^{2+} molar ratio, and EDTA concentration were equal to 5 mM, 4, and 1 mM in 25 minutes, respectively, and the mean efficiency (on the five main surfaces of CIP initial concentration) expected for CIP removal and SIR were 81.83% and 1.39 (gr/M), respectively.

The conflicting objectives problem was modeled by an NSGA-II algorithm to obtain the objectives interaction curve. Figure 5 shows the convergence of the response. As can be seen in the graphs, the response points have a good convergence.

480
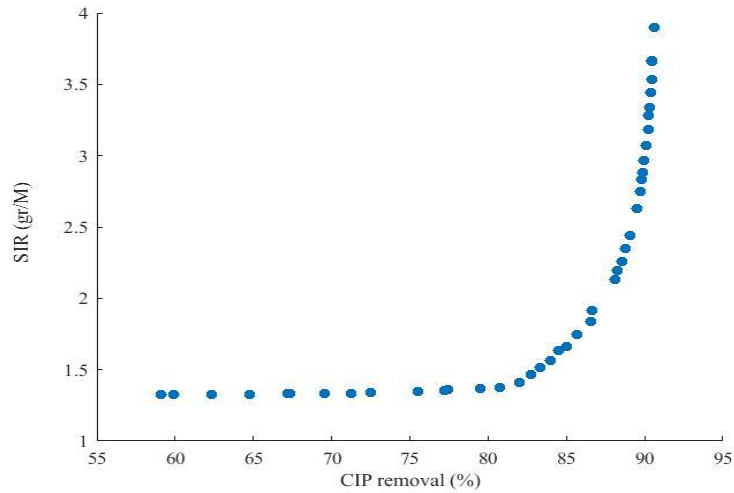
Figure 5. Two-dimensional objectives Pareto front from NSGA-II algorithm

482 Once the optimal solutions are determined by the NSGA-II algorithm, the final step is to select the best

483 alternative according to the importance of the criteria (CIP removal and SIR). The best points are those

484 with maximized CIP removal and minimized SIR functions. For this purpose, a multi-criteria decision-

485 making method (TOPSIS) was used to select the optimal solution, with weights equal to 0.5 for all criteria.

486 Table 6 shows results at the optimal solution, selected by GA and NSGA-II.

487 **Table 6.** Optimal results of the algorithm GA and NSGA-II

Parameters	GA	NSGA-II
Fe^{2+} Concentration (mM)	5	5.94
$[H_2O_2]/[Fe^{2+}]$ mole ratio	4	3.74
EDTA Concentration (mM)	1	0.95
CIP (%)	81.83	83.76
SIR (gr/M)	1.39	1.36

488

489 As shown in Table 6, NSGA-II and GA algorithms have almost similar results and both consider the

490 interaction between conflicting objectives. However, NSGA-II algorithm apparently performed better in

491 the CIP removal model. Therefore, it was concluded that the NSGA-II method might be selected to solve

492 executable problems with higher accuracy and fewer and faster calculations than other multi-objective

493 optimization methods. Also, by comparing RSM-CCD and NSGA-II optimization models, it was concluded

494 that both might predict similar optimal values for variables.

26

4. Conclusions

Determining the operating conditions to optimize the response process is an essential issue in industrial applications. In this study, optimization, modeling, and analysis of the effects of environmental components such as CIP concentration (mg/L), $[Fe^{2+}]$ concentration (mM), $[H_2O_2]/[Fe^{2+}]$ mole ratio, and EDTA concentration (mM) on two main goals, namely, maximizing CIP removal and minimizing SIR, were investigated. The analysis of variance (ANOVA) in a Fenton-like homogeneous process with an EDTA chelating agent showed that all independent variables are effective in CIP removal response, with the initial CIP concentration and EDTA being the most important ones. Also, EDTA and Fe^{2+} concentrations were the most important independent variables on SIR. Accordingly, models with detection coefficients of 0.91% and 0.86 mM were obtained for the rate of CIP removal and the amount of produced SIR sludge, respectively.

Simultaneous optimization results of CIP removal and the amount of produced sludge reduction using RSM showed that under optimal conditions, the values of initial CIP concentration, Fe^{2+} concentration, molar ratio $[H_2O_2]/[Fe^{2+}]$, initial EDTA and reaction time were 14.97 mg/L, 9.18 mM, 3.25, 0.62 mM and 25 min, respectively. Under the optimal conditions, CIP removal rate and the amount of SIR were predicted as 85.18% and 2.24 gr/M, respectively. Also, two validation experiments were performed under these conditions and a close correlation between observed and predicted values was obtained, confirming the models' validity.

Among the two investigated artificial neural networks (RBF and MLP), MLP-ANN could predict the process performance with reliable accuracy (MARE less than 8%). The neural network model had less error compared to RSM model and the overall performance of these models was considered very good.

Multi-objective optimization of the process was performed with two algorithms (GA and NSGA-II). It was concluded that the NSGA-II algorithm performed much better than the GA optimization algorithm according to the weighted sum of normalized targets and the importance of conflicting targets was more

27

519   visible in the NSGA-II algorithm. It is attributed to the NSGA-II algorithm searching the entire decision

520   space as opposed to GA local search for the optimum solution. Comparison of results obtained by multi-

521   objective RSM (RSM-CCD) and NSGA-II optimization models showed that predicted optimal variable

522   values are close in both models and both yield reliable predictions according to ARE criterion.

523

524   **References**

525   Ahari, J.S., Sadeghi, M.T., Zarrinpashne, S. and Irandoukht, A., 2013. Optimization of OCM reactions over

526   Na–W–Mn/SiO_2 catalyst at elevated pressure using artificial neural network and response surface

527   methodology. Sci. Iran., 20(3), 617-625.

528   Al-Shamisi, M., Assi, A. and Hejase, H., 2014. Estimation of global solar radiation using artificial neural

529   networks in Abu Dhabi City, United Arab Emirates. J. Sol. Energy Eng., 136(2).

530   Al Maadheed, S.T.A.A., 2016. Determination of antibiotics and caffeine in hospital wastewater and

531   wastewater treatment plants (WWTPs) in Doha, Qatar (Doctoral dissertation, Qatar University (Qatar)).

532   Ahmadi, S., Mesbah, M., Igwegbe, C.A., Ezeliora, C.D., Osagie, C., Khan, N.A., Dotto, G.L., Salari, M.

533   and Dehghani, M.H., 2021. Sono electro-chemical synthesis of LaFeO3 nanoparticles for the removal

534   of fluoride: Optimization and modeling using RSM, ANN and GA tools. J. Environ. Chem. Eng., 9(4),

535   105320.

536   Aleboyeh, A., Kasiri, M.B., Olya, M.E. and Aleboyeh, H., 2008. Prediction of azo dye decolorization by

537   UV/H_2O_2 using artificial neural networks. Dyes Pigm., 77(2), 288-294.

538   Arab, M., Faramarz, M.G. and Hashim, K., 2022. Applications of Computational and Statistical Models for

539   Optimizing the Electrochemical Removal of Cephalexin Antibiotic from Water. Water, 14(3), p.344.

540

541 Bajpai, S.K., Chand, N. and Mahendra, M., 2014. The adsorptive removal of a cationic drug from aqueous

542   solution using poly (methacrylic acid) hydrogels. Water SA., 40(1), 49-56.

543 Coello, C.A.C., Lamont, G.B. and Van Veldhuizen, D.A., 2007. Evolutionary algorithms for solving multi-

544   objective problems New York: Springer., Vol. 5, 79-104

545 Cámara, M., Ortega, J. and de Toro, F., 2012. Comparison of frameworks for parallel multi-objective

546   evolutionary optimization in dynamic problems. In Parallel Architectures and Bioinspired Algorithms.

547   Springer, Berlin, Heidelberg., 101-123

548 Capriotti, A.L., Cavaliere, C., Piovesana, S., Samperi, R. and Laganà, A., 2012. Multiclass screening

549   method based on solvent extraction and liquid chromatography–tandem mass spectrometry for the

550   determination of antimicrobials and mycotoxins in egg. J. Chromatogr. A., 1268, 84-90.

551 Deb, K., Pratap, A., Agarwal, S. and Meyarivan, T.A.M.T., 2002. A fast and elitist multi-objective genetic

552   algorithm: NSGA-II. IEEE Trans. Evol. Comput., 6(2), 182-197.

553 Desai, K.M., Survase, S.A., Saudagar, P.S., Lele, S.S. and Singhal, R.S., 2008. Comparison of artificial

554   neural network (ANN) and response surface methodology (RSM) in fermentation media optimization:

555   case study of fermentative production of scleroglucan. Biochem. Eng. J., 41(3), 266-273.

556 Ehteshami, M., Zolfaghari, H., Salari, M. and Teymouri, E., 2021. Mespilus germanica (MG) and Tribulus

557   terrestris (TT) Used as Biosorbents for Lead Removal from Aqueous Solutions: Adsorption Kinetics

558   and Mechanisms. Adv. Mater. Sci., 2021. https://doi.org/10.1155/2021/8436632.

559 Elmolla, E. and Chaudhuri, M., 2009. Optimization of Fenton process for treatment of amoxicillin,

560   ampicillin and cloxacillin antibiotics in aqueous solution. J. Hazard. Mater., 170(2-3), 666-672.

561 Elmolla, E.S., Chaudhuri, M. and Eltoukhy, M.M., 2010. The use of artificial neural network (ANN) for

562   modeling of COD removal from antibiotic aqueous solution by the Fenton process. J. Hazard.

563   Mater., 179(1-3), 127-134.

564   Flora, S.J. and Pachauri, V., 2010. Chelation in metal intoxication. Int. J. Environ. Res., 7(7), 2745-2788.

565   Fan, M., Hu, J., Cao, R., Xiong, K. and Wei, X., 2017. Modeling and prediction of copper removal from

566   aqueous solutions by nZVI/rGO magnetic nanocomposites using ANN-GA and ANN-PSO. Sci.

567   Rep., 7(1),1-14.

568   Gadekar, M.R. and Ahammed, M.M., 2019. Modelling dye removal by adsorption onto water treatment

569   residuals using combined response surface methodology-artificial neural network

570   approach. J. Environ. Manage., 231, pp.241-248.

571   Gagnon, C., Lajeunesse, A., Cejka, P., Gagne, F., & Hausler, R., (2008). Degadation of selected acidic and

572   neutral pharmaceutical products in a primary-treated wastewater by disinfection processes. Ozone Sci

573   Eng., 30 :387-92.

574   Haber, F. and Weiss, J., 1934. The catalytic decomposition of hydrogen peroxide by iron salts. Proceedings

575   of the Royal Society of London. Series A-Mathematical and Physical Sciences, 147(861), pp.332-351.

576   He, H. and Zhou, Z., 2017. Electro-Fenton process for water and wastewater treatment. Crit Rev Environ

577   Sci Technol., 47(21), 2100-2131.

578   H Mahdi, M., J Mohammed, T. and A Al-Najar, J., 2021. Removal of Tetracycline Antibiotic from

579   Wastewater by Fenton Oxidation Process. J. Eng. Technol. 39(2), pp.260-267.

580   Jacob, S. and Banerjee, R., 2016. Modeling and optimization of anaerobic codigestion of potato waste and

581   aquatic weed by response surface methodology and artificial neural network coupled genetic

582   algorithm. Bioresour. Technol., 214, 386-395.

583   Kovalakova, P., Cizmas, L., McDonald, T.J., Marsalek, B., Feng, M. and Sharma, V.K., 2020. Occurrence

584   and toxicity of antibiotics in the aquatic environment: A review. Chemosphere., 251, 126351.

585   Kümmerer, K., 2009. Antibiotics in the aquatic environment–a review–part II. Chemosphere., 75(4), 435-

586   441.

587 Kaur, P., Sangal, V.K. and Kushwaha, J.P., 2019. Parametric study of electro-Fenton treatment for real

588   textile wastewater, disposal study and its cost analysis. Int. J. Environ. Sci. Technol., 16(2), pp.801-810.

589 Lapworth, D.J., Baran, N., Stuart, M.E. and Ward, R.S., 2012. Emerging organic contaminants in

590   groundwater: a review of sources, fate and occurrence. Environ. Pollut., 163, 287-303.

591 Lee, C. and Sedlak, D.L., 2009. A novel homogeneous Fenton-like system with Fe (III)–phosphotungstate for

592   oxidation of organic compounds at neutral pH values. J Mol Catal A Chem., 311(1-2), pp.1-6.

593 Li, J., Zhang, K. and Zhang, H., 2018. Adsorption of antibiotics on microplastics. Environ. Pollut., 237,

594   460-467.

595 Li, Y., Li, F., Li, F., Yuan, F. and Wei, P., 2015. Effect of the ultrasound–Fenton oxidation process with

596   the addition of a chelating agent on the removal of petroleum-based contaminants from

597   soil. ESPR., 22(23),18446-18455.

598 Mahmoudpour, M., Gholami, S., Ehteshami, M. and Salari, M., 2021. Evaluation of Phytoremediation

599   Potential of Vetiver Grass (Chrysopogon zizanioides (L.) Roberty) for Wastewater Treatment. Adv.

600   Mater. Sci., 2021. https://doi.org/10.1155/2021/3059983

601 Manyi-Loh, C., Mamphweli, S., Meyer, E. and Okoh, A., 2018. Antibiotic use in agriculture and its

602   consequential resistance in environmental sources: potential public health implications. Molecules.,

603   23(4), 795.

604 Mayer, C. and Takiff, H., 2014. The molecular genetics of fluoroquinolone resistance in Mycobacterium

605   tuberculosis. Molecular Genetics of Mycobacteria. 455-478.

606 Mahamuni, N.N. and Adewuyi, Y.G., 2010. Advanced oxidation processes (AOPs) involving ultrasound

607   for waste water treatment: a review with emphasis on cost estimation. Ultrason Sonochem., 17(6),990-

608   1003.

609   Miao, X., Ma, Y., Chen, Z. and Gong, H., 2018. Oxidative degradation stability and hydrogen sulfide

610   removal performance of dual-ligand iron chelate of Fe-EDTA/CA. Environ. Technol., 39(23), 3006-

611   3012.

612   Messele, S.A., 2014. Homogeneous and heterogeneous aqueous phase oxidation of phenol with fenton-like

613   processes (Doctoral dissertation, Universitat Rovira i Virgili).

614   Messele, S.A., Bengoa, C., Stüber, F.E., Giralt, J., Fortuny, A., Fabregat, A. and Font, J., 2019. Enhanced

615   degradation of phenol by a fenton-like system (Fe/EDTA/H_2O_2) at circumneutral pH. Catalysts, 9(5),

616   p.474.

617   Mooselu, M.G., Liltved, H., Nikoo, M.R., Hindar, A. and Meland, S., 2020. Assessing optimal water quality

618   monitoring network in road construction using integrated information-theoretic techniques. J. Hydrol.,

619   589, 125366.

620   Nandi, S., Mukherjee, P., Tambe, S.S., Kumar, R. and Kulkarni, B.D., 2002. Reaction modeling and

621   optimization using neural networks and genetic algorithms: case study involving TS-1-catalyzed

622   hydroxylation of benzene. Ind. Eng. Chem., 41(9), 2159-2169.

623   Ngan, C.L., Basri, M., Lye, F.F., Masoumi, H.R.F., Tripathy, M., Karjiban, R.A. and Abdul-Malek, E.,

624   2014. Comparison of Box–Behnken and central composite designs in optimization of fullerene loaded

625   palm-based nano-emulsions for cosmeceutical application. Ind Crops Prod., 59, pp.309-317.

626   Neyens, E. and Baeyens, J., 2003. A review of classic Fenton's peroxidation as an advanced oxidation

627   technique. J. Hazard. Mater., 98(1-3), 33-50.

628   Park, D., Cha, J., Kim, M. and Go, J.S., 2020. Multi-objective optimization and comparison of surrogate

629   models for separation performances of cyclone separator based on CFD, RSM, GMDH-neural network,

630   back propagation-ANN and genetic algorithm. Eng. Appl. Comput. Fluid Mech., 14(1), 180-201.

631   Rakhshandehroo, G.R., Salari, M. and Nikoo, M.R., 2018. Optimization of degradation of ciprofloxacin
632   antibiotic and assessment of degradation products using full factorial experimental design by Fenton
633   homogenous process. Glob. Nest J., 20(2), 324-332.

634   Rakić, T., Kasagić-Vujanović, I., Jovanović, M., Jančić-Stojanović, B. and Ivanović, D., 2014. Comparison
635   of full factorial design, central composite design, and box-behnken design in chromatographic method
636   development for the determination of fluconazole and its impurities. Anal. Lett., 47(8), pp.1334-1347.

637   Salari, M., 2021a. Optimisation using Taghuchi method and Heterogeneous Fenton-like Process with
638   Fe_3O_4/MWCNTS Nano-Composites as the Catalyst for Removal an Antibiotic. AANBT., 2(3), 46-53.

639   Salari, M., Rakhshandehroo, G.R., Nikoo, M.R., Zerafat, M.M. and Mooselu, M.G., 2021b. Optimal
640   degradation of Ciprofloxacin in a heterogeneous Fenton-like process using (δ-FeOOH)/MWCNTs
641   nanocomposite. Environ. Technol. Innov., 23, 101625.

642   Speck, F., Raja, S., Ramesh, V. and Thivaharan, V., 2016. Modelling and optimization of homogenous
643   photo-Fenton degradation of rhodamine B by response surface methodology and artificial neural
644   network. Int J Environ Res., 10(4), 543-554.

645   Sarkar, D. and Modak, J.M., 2003. Optimisation of fed-batch bioreactors using genetic algorithms. Chem.
646   Eng. Sci., 58(11), 2283-2296.

647   Salari, M., Rakhshandehroo, G.R. and Nikoo, M.R., 2018. Multi-objective optimization of ciprofloxacin
648   antibiotic removal from an aqueous phase with grey taguchi method. J Water Health., 16(4), 530-541.

649   Salari, M., Rakhshandehroo, G.R. and Nikoo, M.R., 2019. Developing multi-criteria decision analysis and
650   Taguchi method to optimize ciprofloxacin removal from aqueous phase. Environ Eng Manag J.,
651   (EEMJ), 18(7).

652 Salari, M., Rakhshandehroo, G.R. and Nikoo, M.R., 2018. Degradation of ciprofloxacin antibiotic by

653 Homogeneous Fenton oxidation: Hybrid AHP-PROMETHEE method, optimization, biodegradability

654 improvement and identification of oxidized by-products. Chemosphere, 206, 157-167.

655 Salari, M., 2022. Optimization by Box–Behnken Design and Synthesis of Magnetite Nanoparticles for

656 Removal of the Antibiotic from an Aqueous Phase. Adsorp Sci Technol, 2022.

657 Shoorangiz, M., Nikoo, M.R., Salari, M., Rakhshandehroo, G.R. and Sadegh, M., 2019. Optimized electro-

658 Fenton process with sacrificial stainless steel anode for degradation/mineralization of

659 ciprofloxacin. Process Saf. Environ. Prot., 132, 340-350.

660 Talwar, S., Sangal, V.K., Verma, A., Kaur, P. and Garg, A., 2018. Modeling, optimization and kinetic study

661 for photocatalytic treatment of ornidazole using slurry and fixed-bed approach. Arabian Arab J Sci

662 Eng, 43(11), pp.6191-6202.

663 Talwar, S., Verma, A.K. and Sangal, V.K., 2019. Modeling and optimization of fixed mode dual effect

664 (photocatalysis and photo-Fenton) assisted Metronidazole degradation using ANN coupled with genetic

665 algorithm. J. Environ. Manage. 250, p.109428.

666 Talwar, S., Verma, A.K. and Sangal, V.K., 2020. Plug flow approaching novel reactor employing in-situ

667 dual effect of photocatalysis and photo-Fenton for the degradation of

668 metronidazole. Chem. Eng. J., 382, p.122772.

669 Talwar, S., Verma, A.K. and Sangal, V.K., 2021. Synergistic degradation employing photocatalysis and

670 photo-Fenton process of real industrial pharmaceutical effluent utilizing the Iron-Titanium dioxide

671 composite. Process Saf. Environ. Prot. 146, pp.564-576.

672 Torres-Pinto, A., Sampaio, M.J., Teixo, J., Silva, C.G., Faria, J.L. and Silva, A.M., 2020. Photo-Fenton

673 degradation assisted by in situ generation of hydrogen peroxide using a carbon nitride photocatalyst. J.

674 Water Process. Eng., 37, 101467.

675 Usman, M., Hanna, K. and Haderlein, S., 2016. Fenton oxidation to remediate PAHs in contaminated soils:

676   a critical review of major limitations and counter-strategies. Sci. Total Environ., 569, pp.179-190.

677 Vinayagam, R., Dave, N., Varadavenkatesan, T., Rajamohan, N., Sillanpää, M., Nadda, A.K., Govarthanan,

678   M. and Selvaraj, R., 2022a. Artificial neural network and statistical modelling of biosorptive removal of

679   hexavalent chromium using macroalgal spent biomass. Chemosphere, p.133965.

680 Vinayagam, R., Pai, S., Murugesan, G., Varadavenkatesan, T., Narayanasamy, S. and Selvaraj, R., 2022b.

681   Magnetic activated charcoal/Fe_2O_3 nanocomposite for the adsorptive removal of 2, 4-

682   Dichlorophenoxyacetic acid (2, 4-D) from aqueous solutions: Synthesis, characterization, optimization,

683   kinetic and isotherm studies. Chemosphere, 286, p.131938.

684 Vicente, F., Rosas, J.M., Santos, A. and Romero, A., 2011. Improvement soil remediation by using

685   stabilizers and chelating agents in a Fenton-like process. Chem. Eng. J., 172(2-3), 689-697.

686 Wei, R., 2011. Occurrence of veterinary antibiotics in animal wastewater and surface water around farms

687   in Jiangsu Province. Chemosphere., 82: 1408-14.

688 Yamashita, R., Nishio, M., Do, R.K.G. and Togashi, K., 2018. Convolutional neural networks: an overview

689   and application in radiology. Insights Imaging., 9(4), 611-629.

690 Yang, Z.Z. and Moodie, D.R., 2011. Locating urban logistics terminals and shopping centres in a Chinese

691   city. Int. J. Logist. Res. Appl., 14(3), 165-177.

692 Zhou, L., Zheng, W., Ji, Y., Zhang, J., Zeng, C., Zhang, Y., Wang, Q. and Yang, X., 2013. Ferrous-activated

693   persulfate oxidation of arsenic (III) and diuron in aquatic system. J. Hazard. Mater., 263, 422-430.

694